Label-Free Fluorescent Poly(amidoamine) Dendrimer for Traceable and Controlled Drug Delivery

Label-free fluorescent poly(amidoamine) dendrimer for traceable and controlled drug delivery

Journal:	*Biomacromolecules*
Manuscript ID	bm-2019-004945
Manuscript Type:	Article
Date Submitted by the Author:	11-Apr-2019
Complete List of Authors:	Wang, Guoying; Macquarie University Fu, Libing; Macquarie University, Biomedical Sciences K.Walker, Adam; Queensland Brain Institute The University of Queensland Chen, Xianfeng; University of Edinburgh, School of Engineering Lovejoy, David; Macquarie University Hao, Mingcong; Henan University Lee, Albert; Macquarie University, Department of Biomedical Sciences Chung, Roger; Macquarie University, Department of Biomedical Sciences Rizos, Helen; Macquarie University Faculty of Medicine and Health Sciences, Biomedical Sciences Irvine, Mal; Macquarie University, Department of Biomedical Sciences Zheng, Meng; Henan University, School of Life Sciences Liu, Xiuhua; Henan University, Lu, Yiqing; Macquarie University, Physics and Astronomy Shi, Bingyang; Macquarie University, Faculty of Medicine & Health Sciences

Label-free fluorescent poly(amidoamine) dendrimer for traceable and controlled drug delivery

Guoying Wang[a,b], *Libing Fu*[a,b], *Adam Walker* [a,e], *Xianfeng Chen*[f], *David B Lovejoy*[a], *Mingcong Hao*[b], *Albert Lee* [a], *Roger Chung*[a], *Helen Rizos*[a], *Mal Irvine*[a], *Meng Zheng*[b], *Xiuhua Liu** [c], *Yiqing Lu** [b,d], *Bingyang Shi** [a,b]

[a] Department of Biomedical Sciences, Faculty of Medicine & Health Sciences, Macquarie University, Sydney, NSW 2109, Australia

[b] Henan-Macquarie University joint center for Biomedical Innovation, Henan University, Kaifeng, 475001, China

[c] School of Chemical Engineering, Henan University, Kaifeng, 475001, China

[d] Department of Physics and Astronomy, Faculty of Sciences & Engineering, Macquarie University, Sydney, NSW 2109, Australia

[e] Queensland Brain Institute, The University of Queensland, St Lucia, QLD 4072, Australia

[f] School of Engineering, Institute of Bioengineering, The University of Edinburgh, King's Buildings, Mayfield Road, Edinburgh EH93JL, United Kingdom

ABSTRACT

Poly(amidoamine) dendrimer (PAMAM) is well known for its high efficiency as a drug delivery vehicle. However, the intrinsic cytotoxicity and lack of a detectable signal to facilitate tracking have impeded its practical applications. Herein, we have developed a novel label-free fluorescent and biocompatible PAMAM derivative by simple surface modification of PAMAM using acetaldehyde. The modified PAMAM possessed a strong green fluorescence, which was generated by the C=N bonds of the resulting Schiff Bases via n-π^* transition, while the intrinsic cytotoxicity of PAMAM was simultaneously ameliorated. Through further PEGylation, the fluorescent PAMAM demonstrated excellent intracellular tracking in human melanoma SKMEL28 cells. In addition, our PEGylated fluorescent PAMAM derivative achieved enhanced loading and delivery efficiency of the anticancer drug doxorubicin (DOX) compared to the original PAMAM. Importantly, the accelerated kinetics of DOX-encapsulated fluorescent PAMAM nanocomposites in an acidic environment facilitated intracellular drug release, demonstrating comparable cytotoxicity to that of the free-form doxorubicin hydrochloride (DOX·HCl) against melanoma cells. Overall, our label free fluorescent PAMAM derivative offers a new opportunity of traceable and controlled delivery for DOX and other drugs of potential clinical importance.

KEY WORDS

Label-free fluorescence, PAMAM, Drug delivery, Intracellular tracking, Doxorubicin

1 INTRODUCTION

Dendrimers, a notable class of highly branched synthetic macromolecules, hold great promise for developing nano-sized drug delivery systems (DDS) with specially designed targeting functions and controlled release capabilities for therapeutic applications in cancer, neurodegeneration and cardiovascular disease[1-4]. In particular, poly(amidoamine) (PAMAM) dendrimers have attracted increasing interest as excellent candidates for DDS, due to their controllable molecular size, monodispersity and abundant surface functional groups[5-8]. To facilitate mechanistic studies and optimization of carrier design and delivery efficiency, it is practically required that the DDS have detectable signals to be traced intracellularly and in real time[9, 10]. However, the pristine PAMAM dendrimer is a non-fluorescent macromolecule, although, fluorescent labelling can be used to overcome this problem[11], these approaches result in changes in surface charge, solubility, biocompatibility and other physicochemical properties as well as limiting the potential for further surface modification and functionalization. Additionally, the cost, biosafety and disposal of labelling fluorescent materials present other problems in their practical applications[12, 13]. In last few years, researchers have reported several non-traditional intrinsic blue luminescence PAMAM dendrimers for biological applications and demonstrated that the emission intensity can be enhanced by lowering pH[14-16], oxidation protocols[14, 17] or surface chemistry engineering[16]. In particularly, surface chemistry engineering is deemed to be the most realistic strategy for designing high emission intensity materials since lowing pH or oxidation protocols can be fatal for *in vivo* systems due to protein denaturation and ROS generation[16]. Plenty of micro molecules such as mannose[18], 3-aminobenzeneboronic acid[19] and 4-carbomethoxy pyrrolidone[20] have been successfully applied to PAMAM to fabricate high inherent blue fluorescent PAMAM dendrimers with excellent biocompatibility and imaging capabilities. However, those chemistry engineered blue fluorescent dendrimers usually require UV excitation, which poses major limitations in its application since UV is

harmful to living cells and biological systems[21]. Also, the cells and tissues may become auto-fluorescent when excited by UV/Vis radiation of suitable wavelength, which may also hinder the practical application of blue fluorescent PAMAM dendrimers in biological system[22]. To our knowledge, relatively little research has reported other colored (green, red) inherent fluorescent PAMAM. Therefore, it remains a crucial challenge to develop powerful label-free fluorescent PAMAM dendrimer for PAMAM-based DDS.

Herein, we developed a label-free green fluorescent PAMAM dendrimer by surface modification of pristine PAMAM with acetaldehyde to generate new traceable and controllable DDS (Scheme 1). Through the aldehyde-ammonia reaction, the terminal primary amino groups in PAMAM were replaced by Schiff base terminals. The modified PAMAM exhibited strong green fluorescence with a maximum emission at 507 nm and maximum excitation at 485 nm due to the n-π* transition of the C=N bonds in the resulting Schiff bases[23]. Attractively, this fluorescence behaviour was pH-independent, which was highly desirable for applications in biological systems. Furthermore, the intrinsic cytotoxicity of PAMAM, caused by high positive charge of the terminal amines, was substantially decreased[24], since replacement of amines by Schiff base terminals neutralized the overall surface charge. To ensure stability of the label-free fluorescent PAMAM in biological media, PEGylation was performed to introduce steric hindrance that prevented aggregation of the nanocarriers[25-27], and afforded excellent biocompatibility in different cell lines. Traceability of the fluorescent PAMAM was also demonstrated in cells using confocal microscopy and flow cytometry. Furthermore, a model drug, doxorubicin (DOX),was encapsulated into our new nanocarriers by a precipitation method, and drug release kinetics were evaluated at different pH values[28]. To evaluate cancer cell uptake and therapeutic efficacy, SKMel28 cells were used. Our optimized nanocomposites showed higher drug uptake efficacy and better therapeutic efficacy compared to hydrophobic DOX and PAMAM G5/DOX (G5/DOX) composites, respectively. These results demonstrate

that this newly developed modified PAMAM is an improved DDS with potential clinical applicability.

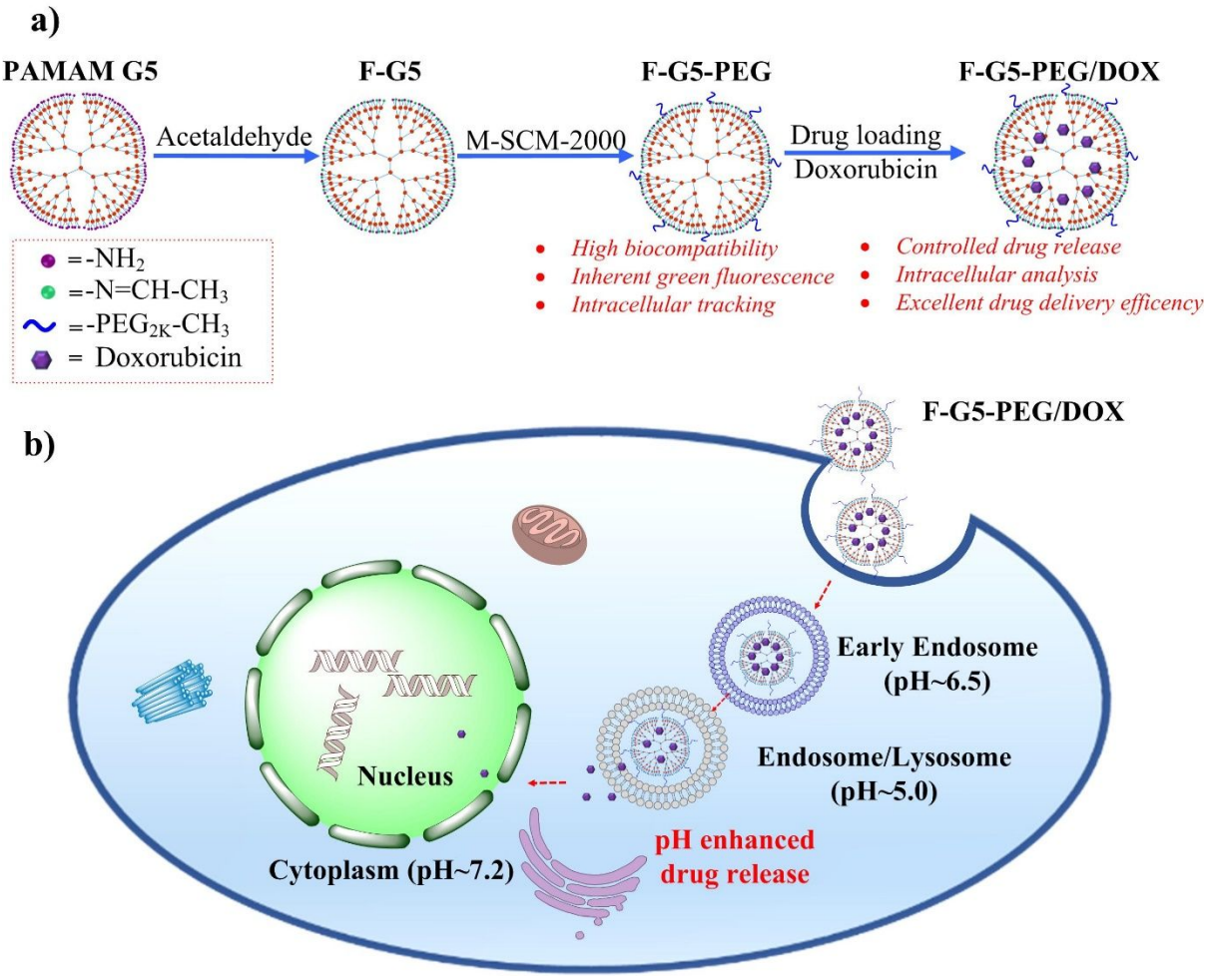

Scheme 1. (a) A schematic description of preparing label free fluorescent poly(amidoamine) dendrimer (F-G5-PEG) and its properties for drug delivery. (b) Intracellular behavior of DOX loaded F-G5-PEG.

2 Materials and methods

2.1 Materials

Ethylenediamine core amine-terminated generation 5 PAMAM dendrimers (G5), acetaldehyde, triethylamine (TEA) and doxorubicin hydrochloride (DOX·HCl) were

purchased from Sigma-Aldrich (NSW, Australia). Methoxy-PEG-Succinimidyl Carboxymethyl Ester (M-SCM-2000; Mw 2000) was purchased from Jenkem Technology (Beijing, China). Amicon® Ultra Centrifugal Filters (10 KD) were purchased from Merck Millipore (VIC, Australia). Dulbecco's Modified Eagle's Medium (DMEM) was purchased from Thermo Fisher Scientific (NSW, Australia), Endothelial Cell Growth Basal Medium-2 (EBM-2) was purchased from Lonza (Melbourne, Australia). VECTASHIELD® mounting medium was purchased from Vector Laboratories (US). (3-(4,5-dimethylthiazol-2-yl)-2,5-diphenyltetrazolium bromide (MTT) was purchased from Life Technologies (NSW, Australia). Other routine chemicals were obtained from Sigma-Aldrich and used as received. The water used in all the experiments was purified using a Milli-Q Plus 185 water purification system (Millipore) with a resistivity higher than 18 MU cm.

2.2 Synthesis of label-free Fluorescent PAMAM G5

The label-free fluorescent PAMAM G5 (F-G5) was synthesized by the reaction of acetaldehyde with amine-terminated G5 at room temperature. G5 (100 mg; 7 mmol) was dissolved in Milli-Q water (10 mL) and adjusted to pH 10 using NaOH solution (0.1 M). Acetaldehyde (in excess) was added dropwise to the G5 solution. The reaction mixture was protected from light and stirred at room temperature for 8h, followed by centrifugation using Amicon® filters at 4500 rpm for 30 min to remove any unreacted acetaldehyde. The purification process was repeated 3 times. The purified solution of F-G5 dendrimer was stored at 4 ^{o}C for further use.

2.3 PEGylation of F-G5

The prepared F-G5was covalently conjugated with M-SCM-2000 via an NHS ester coupling reaction, with the feed molar ratio of 1:30. M-SCM-2000 (2.1 μmol) dissolved into 5 mL water, to which 0.07 μmol F-G5 was added quickly. The mixture was kept at room temperature and

magnetically stirred for 4 h, followed by centrifugation using Amicon filters (4500 rpm for 30 min; repeated 4 times) to remove any unreacted M-SCM-2000. The purified solution of PEGylated F-G5 (F-G5-PEG) was stored at 4 ^{o}C for further use.

2.4 Qualification analysis of F-G5 and F-G5-PEG

Qualification analysis of F-G5 and F-G5-PEG was performed by NGC™ Medium-Pressure Liquid Chromatography Systems. Briefly, 0.5 mL G5, F-G5 or F-G5-PEG (1mg/mL in PBS, pH=7.4) was analysed by the gel filtration using an Enrich^{TM}SEC650 (Bio-Rad) column and NGC purifier (Bio-Rad). Bovine Serum Albumins (BSA, Sigma, MW~ 66K) was used as reference protein. 0.1M PBS (pH=7.4) containing 5% glycerol was used as elution buffer.

2.5 Encapsulation of DOX within F-G5-PEG

DOX was encapsulated inside F-G5-PEG using a solvent-displacement (nanoprecipitation) method slightly modified from literature[29]. F-G5-PEG (0.07 μmol) was dissolved in 3 mL water, while 0.7 μmol DOX·HCl was dissolved in 0.4 mL methanol and neutralized sequentially with 3.5, 5.25, 7μmol triethylamine (TEA) to generate hydrophobic DOX. The hydrophobic DOX solution was then added dropwise into F-G5-PEG solution and magnetically stirred overnight to evaporate excess methanol and TEA. The F-G5-PEG/DOX solution was centrifuged at 10,000 rpm for 10 min, to precipitate non-encapsulated free DOX (as free DOX is water insoluble). The precipitation was collected and dissolved into 5 mL methanol, followed by quantity analysis based on the DOX absorbance intensity at 480 nm via UV-visible measurement. G5/DOX nanocomposites were also prepared using the same protocol with the same molar ratio of G5 to DOX.

2.6 Characterisation

Transmission electron microscopy (TEM) was carried out using a CM10 (Philips) system at an acceleration voltage of 120 kV. F-G5-PEGwas diluted to 0.5 mg/ml in Milli-Q water and sonicated for 10 min, dropped onto carbon-coated copper grids, followed by negative staining using 2% Uranyl Acetate. UV-vis absorption spectra were recorded on a UV-2600 spectrophotometer (Shimadzu, Japan). Fluorescent emission and excitation spectra were recorded on a Fluorolog spectroscopy (Horiba, Australia). Fourier transform infrared (FTIR) spectra were taken on a NICOLET 6700 FTIR spectrometer (Thermo Scientific, Australia) at room temperature. The particle sizes and zeta potentials were measured at room temperature using a Zetasizer Nano ZS (Malvern, Australia) equipped with the ZET 5104 cell. 1H Nuclear Magnetic Resonance (NMR) experiments were recorded using a 400 MHz Bruker NMR in D_2O.

2.7 Kinetic Release Study

F-G5-PEG/DOX nanocomposites and free DOX (50 μg equivalent DOX in 2 mL phosphate buffered saline (PBS), pH 7.4, 6.0 or 5.0) were placed in a dialysis bag with molecular weight cut-off (MWCO) of 10,000, hermetically tied, and suspended in 8 mL PBS buffer (pH 7.4, 6.0 or 5.0). The entire system was kept in a constant-temperature vibrator at 37 ^{o}C. Then, at each predetermined time point, 0.2 mL dialysis buffer was removed for measurement, and 0.2 mL PBS (at the corresponding pH) was added back to keep the total volume of the dialysis buffer constant. The released DOX was quantified by a microplate reader (PHERAstar FS, Australia) that measured the DOX fluorescence (λex = 480 nm, λem = 580 nm). The cumulative release (Cr) of DOX at each time point was obtained according to the equation

$$Cr = Wt/Wtot \times 100\%$$

where Wt and Wtot are the cumulative amount of released drug at time t and the total amount of encapsulated drug in the nanocomposites used in dialysis, respectively.

2.8 Cell Culture

SKMel28 cell line was obtained from the American Type Culture Collection (ATCC). Cells were cultured in DMEM supplemented with 10% fetal bovine serum (FBS, Sigma-Aldrich), 20 mM 4-(2-hydroxyethyl)-1-piperazineethanesulfonic acid (HEPES, Sigma-Aldrich), 4 mM L-Glutamine (Sigma-Aldrich), 100 U/mL penicillin, and 100 U/mL streptomycin (Life Technologies). hCMEC/D3 cell line was obtained from ATCC. Cells were cultured in EMB-2 medium (Lonza, Melbourne) supplemented with 5% FBS, 10 mM HEPES, 100 U/mL penicillin, and 100 U/mL streptomycin and 1 ng/mL basic fibroblast growth factor (Bfgf, ThermoFisher). HEK293 and NSC34 cell lined were obtained from ATCC. Cells were cultured in DMEM supplemented with 10% fetal bovine serum, 100 U/mL penicillin, and 100 U/mL streptomycin. Cultures were maintained at 37 ^{o}C in a wet incubator with 5% CO^2, and the medium was replaced every 3 days.

2.9 Cytotoxicity Test

To test biocompatibility, SKMel28, hCMEC/D3, HEK293 and NSC34 cells were cultured in 96-well plates at density of 5000 cells/well and allowed to adhere overnight at 37 ^{o}C in a humidified 5% CO^2-containing atmosphere. Growth media were replaced with media containing G5, F-G5, or F-G5-PEG. The cells were then incubated for 48 h before 20 μL MTT (5.0 mg/mL in PBS) was added to each well and further incubated for 4 h at 37 ^{o}C. The media was then removed and 150 μL of dimethyl sulfoxide (DMSO) was added to each well to ensure complete solubilization of formazan crystals before cell viability was determined by absorption at 560 nm.

To test therapeutic efficacy, SKMel28 cells were cultured in 96-well plates at density of 5000 cells/well and allowed to adhere overnight at 37 ^{o}C in a humidified 5% CO^2-containing atmosphere. Growth media were replaced with DMEM containing DOX·HCl, DOX (TEA-treated), G5/DOX or F-G5-PEG/DOX at equivalent DOX concentrations range from 0.1 to 5 μg/mL. The cells were then incubated for 48 h, followed by MTT assay as described above.

2.10 Intracellular Tracking of F-PAMAM

SKMel28 cells were seeded at a concentration of 1×10^5 cells/well in 6-well plates containing slide cover glasses (24×24 mm), and cultured at 37 ^{o}C for 24 h. F-G5-PEG was added to the cell culture media to obtain a final concentration of 50 μg /mL for each well, and cells further incubated at 37 ^{o}C for 2, 4, 8 or 24 h. Cells were then washed with PBS followed by adding 1 mL Hoechst 33342 solution (Thermofisher, 1:2000 in PBS) and incubated for 10 minutes (protected from light). After Hoechst staining, cells were washed with PBS again and stained with Cytopainter (Abcam, ab176827) following the manufacturer's protocol. Live cell imaging was performed using a Zeiss LSM 880 laser-scanning confocal microscope.

2.11 Intracellular Drug Delivery

Intracellular drug delivery was assessed using a combination of cellular imaging and flow cytometry. For cellular imaging, SKMel28 cells were seeded at a concentration of 1×10^5 cells/well in 6-well plates containing glass slide covers and cultured at 37 ^{o}C for 24 h. Next, DOX·HCl, DOX (TEA-treated), G5/DOX or F-G5-PEG/DOX were added to culture media to obtain a final DOX concentration of 2.5 μg/mL. Cells were then incubated at 37 ^{o}C for 4 h, followed by washing with PBS (x 3) to remove non-cell incorporated drug. Subsequently, cells were fixed with 4 % paraformaldehyde solution and treated with VECTASHIELD® mounting

medium with DAPI for 10 min at room temperature. Cells were imaged by a Zeiss LSM 880 laser-scanning confocal microscope.

For flow cytometry, SKMel28 cells were seeded at a concentration of 1×10^5 cells/well in 6-well plates and cultured at 37 °C for 24 h. Next, DOX·HCl, DOX (TEA-treated), G5/DOX or F-G5-PEG/DOX were added to culture media to obtain a final DOX concentration of 2.5 μg/mL. Cells were then incubated at 37 °C for 4 h, followed by washing with PBS (x3) to remove non-cell incorporated drug. Subsequently, cells were detached by trypsin, collected and concentrated, and then fixed with 4 % paraformaldehyde at 4 °C overnight. The cells were analysed by a flow cytometer (BD LSR Fortessa X-20, Australia) using FITC and PE channels to quantify the amounts of F-PAMAM and DOX, respectively, in individual cells. Quantification was performed using standardized reference solutions of F-G5-PEG and DOX·HCl.

2.12 Statistical Analysis

One-way ANOVA was performed using Origin 8.0 software to compare the cytotoxicity of cells treated with different materials. The significance level was set as 0.05, and the data were indicated with (**) for $p<0.01$ and (***) for $p<0.001$. Data are expressed as the mean ± standard deviation. Each experiment was performed in triplicate.

3 RESULTS AND DISCUSSION

3.1 Physical and Optical Properties of F-PAMAM and PEGylated F-PAMAM

G5 PAMAM dendrimer was selected for the synthesis of label-free fluorescent dendrimer due to its relative small size (5.4 nm, theoretical value), monodispersity, large internal cavity and numerous functionable amine groups[30, 31]. As shown in schematic 1, the label free fluorescent PAMAM (F-G5) was fabricated by simple surface modification using

acetaldehyde. After 8 h reaction the colorless PAMAM turned to brown (Fig S1), indicating successful formation of Schiff base[12, 32, 33]. PEG (M-SCM-2000) was then conjugated to the surface of F-G5 by classical esterification between N-hydroxysuccinimide (NHS) ester and primary amino groups contained in F-G5. The F-G5 and PEGylated F-G5 (F-G5-PEG) were further characterized by TEM, DLS, FTIR, Liquid Chromatography and 1H NMR.

TEM images in Fig 1a and Fig S1 showed that F-G5-PEG had a relative uniform particle size of approximately 22 nm while G5 had a particle size of approximately 16 nm in water and approximately 5 nm in methanol. The size of nanoparticles was also acquired with DLS measurement. As shown in Fig 1b, the initial size of G5 was 6.6±0.4 nm (Close to theoretical value). After aldehyde modification, the size of F-G5 changed to 5.1±1.1nm, which was smaller than G5. After PEGylation the size of F-G5-PEG increased to 9.8±0.6 nm, which was mainly caused by the grafting of PEG chain. When compared the TEM results (sample prepared in water) with DLS, we found that the size of G5 and F-G5 from TEM was significantly larger than the number size distribution of DLS and theoretical value, the increased size may be caused by the formed non-uniform particle deposition and particle aggregation of dendrimers by the hydrogen interaction in the aqueous solution during drying step[34, 35]. The TEM image of G5 in methanol was around 5 nm (Fig S1) (close to theoretical value) might be an evidence of the above hypothesis. We further analysed the zetapotential by DLS, as seen in Fig 1c, compared with G5, the zeta potential of F-G5/F-G5-PEG showed a significant charge decrease from +28.2 to approximately +4.8 mV. This decreased surface charge was likely primarily due to the replacement of amino groups with non-charged Schiff base terminals and mPEG.

FTIR was next used to characterize the surface functionalization of F-G5 and F-G5-PEG. As displayed in Fig S2, the peaks at 2970, 2873 and 1374 cm^{-1} indicated the presence of -CH_3 groups, suggesting the successful introduction of the Schiff base (-N=CH-) structure on the

PAMAM surface. The peaks at 2880 and 1098 cm^{-1} indicated the presence of C-O-C and confirm the successful conjugation of PEG on the surface of label free fluorescent dendrimer. The absorption peaks due to adsorbed H_2O around 1623 cm^{-1} may potentially overlap with the absorption peaks of -N=C- group and amide I, which are normally observed at 1615~1700 cm^{-1}.

The chemical structure of each dendrimer product and intermediate was also characterized by1H NMR spectroscopy. The spectra of F-G5 and F-G5-PEG were collected to further confirm the successful introduction of various functional groups to the G5 dendrimer. As shown in Fig S3, the chemical shifts of F-G5 at 1.83 and 8.37 ppm were assigned to $-CH_3$ and -N=CH- groups respectively, demonstrating the successful incorporation of the Schiff base structure to PAMAM G5. As calculated from NMR spectrum, around 31.7% amino groups were replaced by $-N=C-CH_3$ groups. The chemical shifts of F-G5-PEG at 3.63 ppm were assigned to $-CH_2-CH_2-$ repeat segments and indicate the successful conjugation of PEG on the surface of F-G5. The chemical shift peak of F-G5-PEG at 2.71 ppm assigned to -NHS was no longer detected, indicating that the NHS had completely reacted with F-G5. However, the chemical shift peak of F-G5-PEG at1.83 and 8.37 ppm was significantly decreased, that's likely because the plenty of PEG chain decreased the sensitivity of 1H NMR. The structure change was further characterized by fluorescent spectrophotometer.

As shown in Fig 1d, our developed PAMAM exhibited green fluorescence due to the n-π* transition of the C=N bonds in the formed Schiff bases, showing similar excitation and emission spectra as our previously reported acetaldehyde modified-cystine (AC)[12]. No emission was detected with the original G5 at 485 nm excitation (Fig S5), suggesting that the fluorescence of F-G5-PEG was only due to the formation of the C=N bonds in the formed Schiff bases. We further tested the fluorescence intensity of F-G5-PEG at three different pH

values (pH 7.4, 6.0, and 5.0) and verified that the fluorescence of F-G5-PEG was pH-independent (Fig S4), suggesting that our label free fluorescent PAMAM could be generally applied to biological systems since the fluorescence will not be adversely affected by differing pH levels present in sub-cellular organelles. The long-term stability assay (shown in Fig S4) demonstrated a marginal fluorescence intensity reduction during the first 48 h (~5%) followed by a ~20% fluorescence intensity reduction after 5 days' continuous incubation, which suggested that this label-free fluorescent PAMAM maintains excellent biological environmental stability. We further compared the fluorescence intensity of F-G5 and F-G5-PEG at the same molar concentration (Figure S6b) and found that the PEGylation only slightly affect the fluorescent properties (less than 5%), suggesting that the PEGylation of F-G5 wouldn't change the Schiff base structure. The sufficient fluorescence intensity of F-G5-PEG makes it an excellent inherent fluorescent material for further biological applications.

The molecular size of G5, F-G5 and F-G5-PEG was further analyzed by size exclusion chromatography (SEC) with ENrich^{TM}SEC650 High-Resolution Size Exclusion Columns. We used BSA as a reference macromolecular with the number size distribution of 8.1±0.9 nm (acquired by DLS in PBS). As shown in Fig 2, the elution time of G5 was slightly later than that of BSA and earlier than F-G5, indicating that the molecular size of G5, F-G5 were following the order that BSA (8.1 nm) >G5>F-G5. The elution time of F-G5-PEG was slightly earlier than that of BSA, which was mainly because the conjugated PEG increased the total molecular size of F-G5. The results of SEC were consistent with the DLS results, which implies that the G5, F-G5, F-G5-PEG were most likely dispersed in PBS buffer as single molecular.

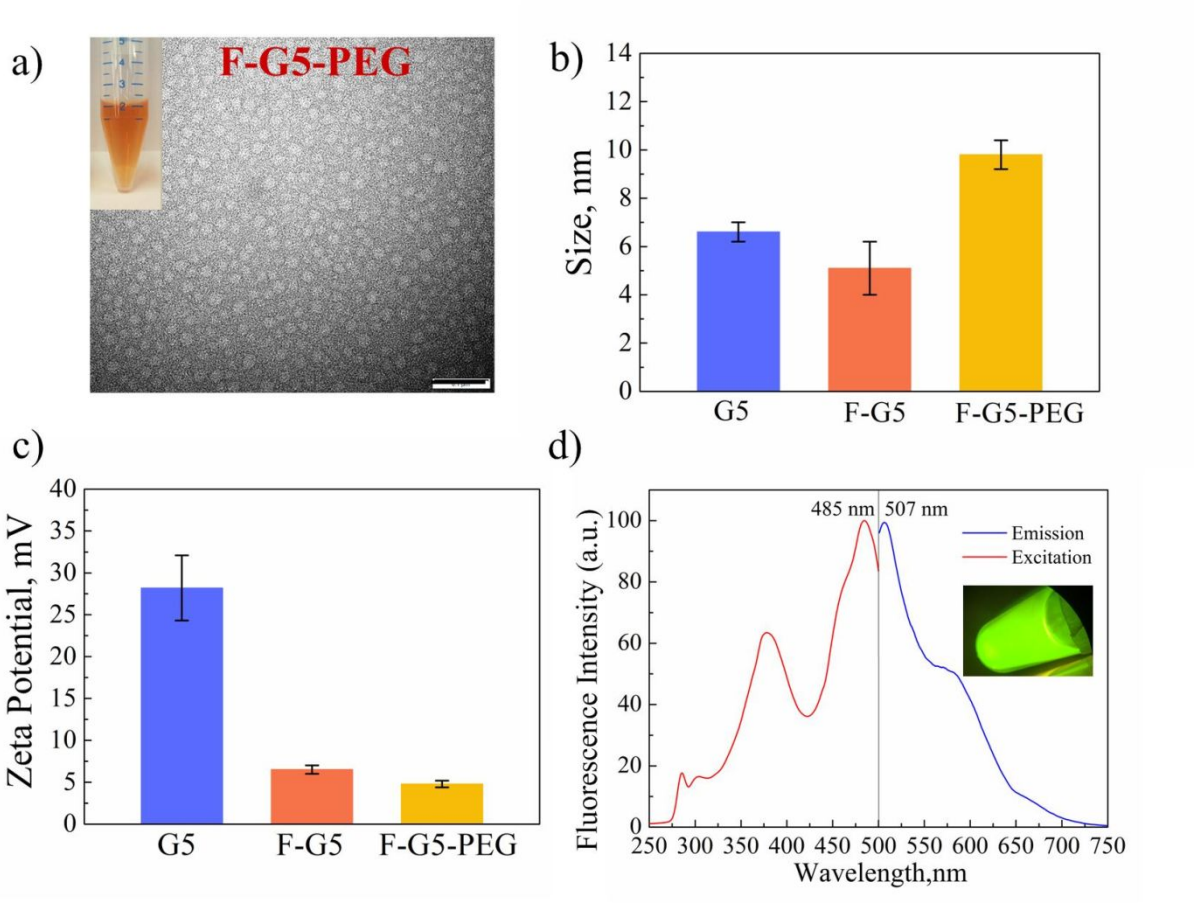

Figure 1. The physical and fluorescence characteristics of modified PAMAM, (a) TEM image of F-G5-PEG in aqueous solutions (The insets showed the digital images of samples), Bar = 0.1 μm; (b) The size distribution of G5, F-G5 and F-G5-PEG by DLS by number distribution (in PBS); (c) The zetapotential of G5, F-G5 and F-G5-PEG by DLS (in PBS); (d) The excitation and emission spectra of F-G5-PEG (The insets showed the fluorescent image of F-G5-PEG under 485 laser excitation).

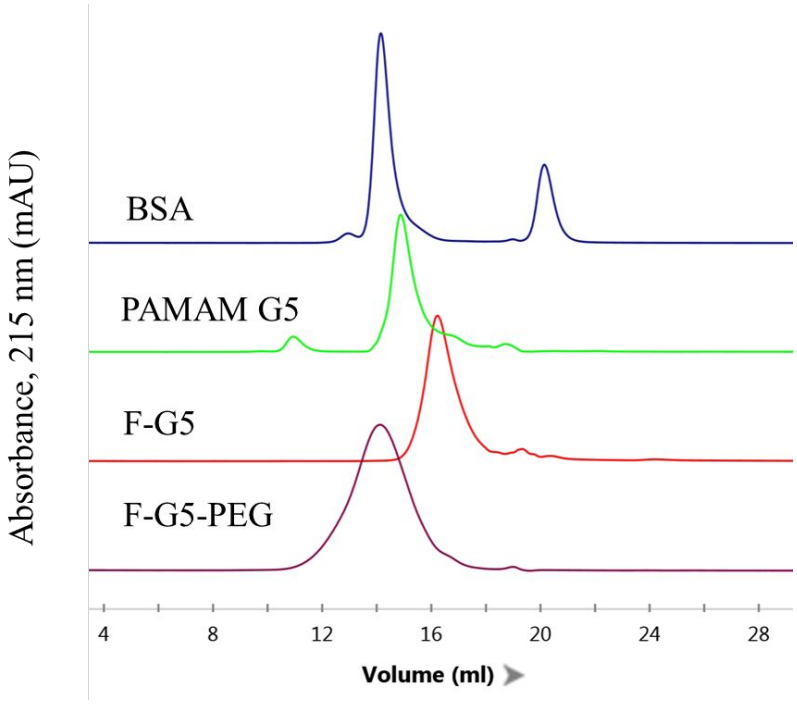

Figure 2. Chromatograms of PAMAMG5, F-G5, F-G5-PEG and BSA by NGC™ Medium-Pressure Liquid Chromatography Systems. The system elution speed was 1 mL/min.

3.2 Biocompatibility of F-PAMAM and PEGylated F-PAMAM

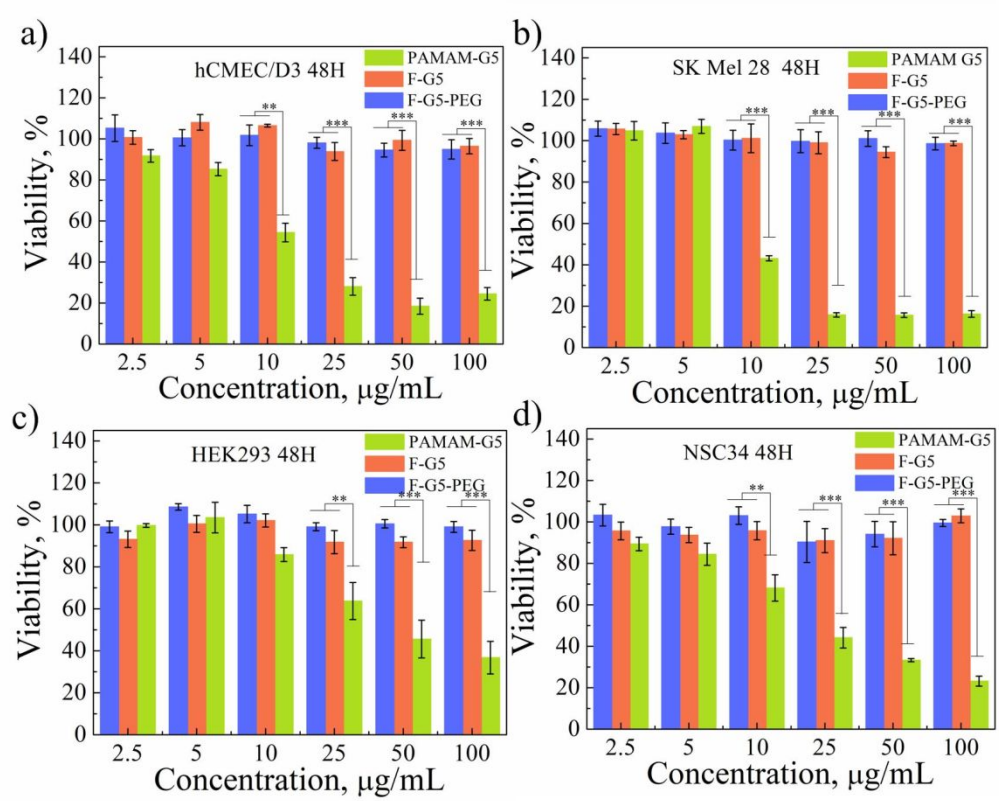

Figure 3. Biocompatibility of modified PAMAM. Cellular viability of (a) hCMEC/D3, (b) SKMel28, (c) HEK293, (d) NSC34 cell lines were treated with cationic PAMAM G5, F-G5 and F-G5-PEG at the concentration range from 2.5 to 100 μg/mL. (***, $p<0.001$, **, $p<0.01$)

In DDS, the nanocarriers should be biocompatible with healthy cells. The biocompatibility of G5, F-G5, F-G5-PEG was evaluated using MTT assays in four different cell lines in the concentration range of 2.5~100 μg/mL. As shown in Fig 3a-d, after 48 h incubation, a remarkable decrease in the cytotoxicity of the cationic PAMAM dendrimers was noted when cells were exposed to the F-G5 and F-G5-PEG, indicated by the average cell viabilities of four cell lines of above 90%, even at the highest concentration of 100 μg/mL. In great contrast, commercial G5 showed significant cytotoxicity to all cell lines, revealed by the low cell viability of below 50% at concentrations of over 10 μg/mL for hCMEC/d3 and SKMel28 cells, 25μg/mL for NSC34 and 50 μg/mL for HEK293. The intrinsic cytotoxicity of PAMAM was usually caused by the high positive charges of dense terminal amines[36]. After acetaldehyde modification amines from PAMAM were replaced by Schiff base terminals and mPEG that neutralized the overall surface charge and resulted in a significant zeta potential decrease (Fig 1c), thereby substantially alleviated cytotoxicity. These results suggested that the novel F-G5 and F-G5-PEG were potentially safe for biological application.

3.3 Fluorescence tracking of F-G5-PEG *in vitro*

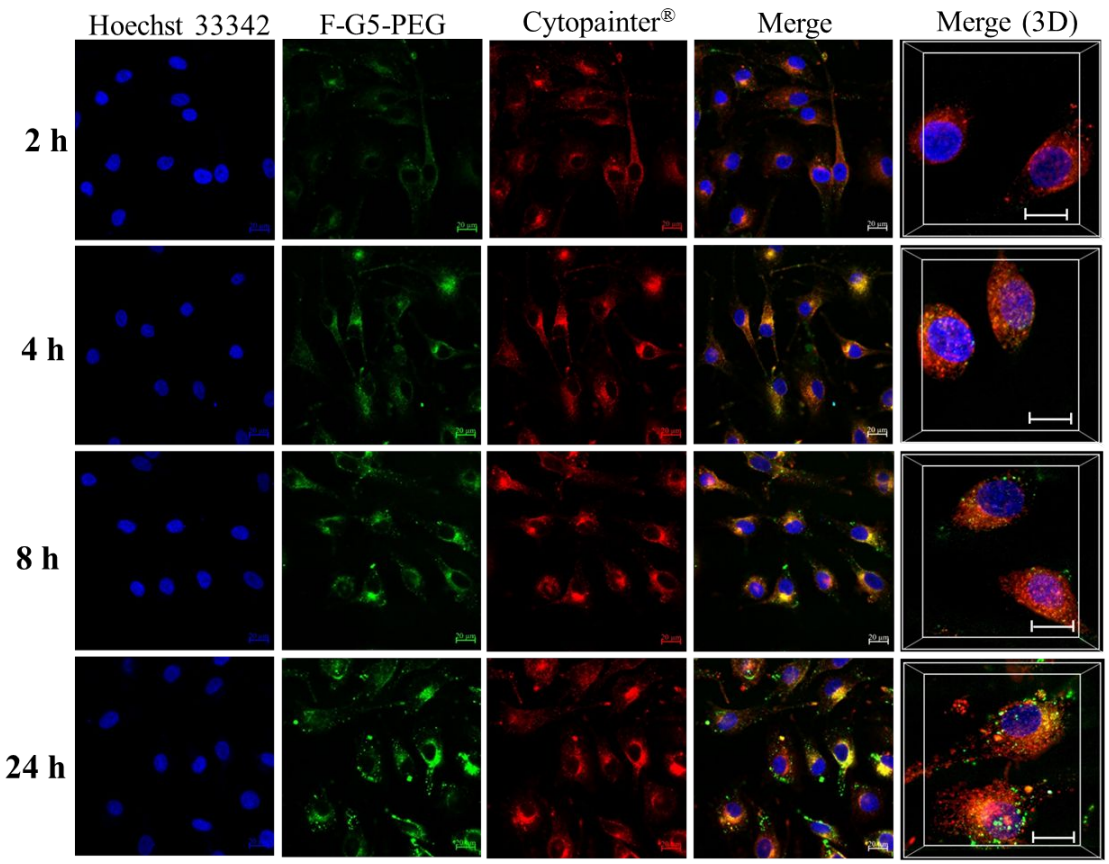

Figure 4. Intracellular tracking of F-G5-PEG (nanocarrier) was assessed in SKMEL28 cell line by confocal microscopy. Live cell imaging was taken at 2, 4, 8, 24 h intervals after incubation. 488 and 545 nm laser excitation were used for detecting Hoechst and Cytopainter. Scale bar = 20 µm.

The intracellular microenvironment-responsive behaviour of F-G5-PEG was monitored at different time intervals using fluorescence microscopy. As shown in Fig 4, after 2 h incubation, very weak green fluorescence signal was obtained. As the incubation period increased to 4 h, green fluorescent spots started to be observed, indicating some complexes have entered cells through endocytosis. With further prolonged incubation time to 24 h, very bright green fluorescence images were obtained, indicating enhanced cell loading. To evaluate the subcellular localization of F-G5-PEG, the cells were stained with Cytopainter® followed the manufacturer's protocol. As seen in Fig 4, at the time point 2, 4 and 8 h, the green signal co-

localization with red signal very well, indicating that the F-G5-PEG was mainly accumulated in lysosome after endocytosis. After 24 h incubation, some F-G5-PEG formed to bright green granules around cell edge, which may be caused by the exocytosis of those granules. However, after 24 h incubation, most of F-G5-PEG was still co-localization with lysosome. These studies suggested that the strong green signals emitted by F-G5-PEG could potentially be used as a tool for intracellular real-time tracking and also for exploring cellular uptake mechanisms.

3.4 Drug Loading and Release

Table 1. Drug encapsulation efficiency and physical properties of G5/DOX and F-G5-PEG/DOX compositions

Sample	TEA:DOX·HCl (mol:mol)	Size[a], nm	Zeta, mV	EE[b], %	LE[c],%
G5/DOX	5:1	/	/	78.6±4.1	13.6±0.7
 F-G5-PEG/DOX-1	5:1	59.5±7.3	6.5±0.8	94.5±2.8	7.3±0.2
 F-G5-PEG/DOX-2	7.5:1	81.9±2.2	6.3±0.6	91.2±2.3	7.0±0.2
 F-G5-PEG/DOX-3	10:1	127.9±1.6	8.2±1.0	84.5±3.6	6.5±0.3

a: Statistics by Z-average

b: EE=Encapsulation efficiency (EE) $=\frac{\mathrm{Wo}}{\mathrm{Wt}} \times 100$, Wt is the total DOX weight used for drug loading and Wo is the weight of encapsulated DOX, respectively.

c: LE= drug loading efficiency (LE)$=\frac{\mathrm{Wo}}{\mathrm{Wt}+\mathrm{Wp}} \times 100$, Wp is the total PAMAM weight used for drug loading.

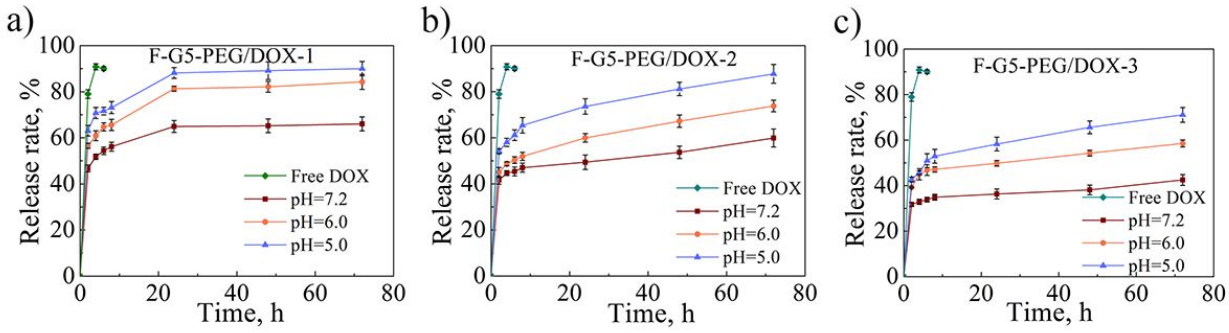

Figure 5. Drug release profile of (a) F-G5-PEG/DOX-1, (b) F-G5-PEG/DOX-2 and (c) F-G5-PEG/DOX-3 in PBS buffer solution with different pH value. Free DOX was used for comparison.

DOX was efficiently encapsulated into F-G5-PEG using a solvent-displacement (precipitation) method. Typically, TEA (Triethylamine) was used to neutralize DOX hydrochloride so that it could be loaded inside the PAMAM hydrophobic cavity[37]. A simple method to achieve high doxorubicin loading in biodegradable polymersomes was previously reported and demonstrated that pH conditions had a strong influence on drug loading capacity and release[38]. Similarly, we used a highly volatile organic base (TEA) to control drug loading by modulating pH conditions. We also explored the effect of molar ratio TEA to DOX·HCl, using 5:1, 7.5:1, 10:1 as F-G5-PEG/DOX-1, -2, -3 respectively. The size and zetapotential of drug loaded nanoparticles were measured with DLS. As shown in Table 1, after drug loading, the size of F-G5-PEG/DOX composites increased dramatically compared with the carrier F-G5-PEG. Meanwhile, a higher TEA to DOX·HCl molar ratio resulted in a larger particle size. No obvious change in zetapotential were detected for all F-G5-PEG/DOX compositions, compared to the drug carrier F-G5-PEG. Presumably, DOX mostly accumulated inside the PAMAM. In our study, non-PEGylated F-G5 was also used to load DOX. However, the F-G5/DOX system was not stable in serum-containing medium and precipitation was evident by upright microscopy (Olympus). Additionally, a large size increase was also detected by DLS

(Table S1) after mixing F-G5/DOX with 10% serum, reflecting the very smooth surface of non-PEGylated F-G5/DOX. The smooth surface of F-G5/DOX composites and extremely low surface charge significantly impaired steric stability, leading to aggregation of F-G5/DOX in serum-containing media[39]. However, with PEGylation, the F-G5-PEG/DOX system was stable in serum-containing media, and no increased particle size were detected by DLS (Table S1) during the observation period. These results were consistent with the use of PEG to improve steric hindrance and enhanced material stability in biological fluids[40].

Drug loading efficiency was determined by measuring the precipitated un-loaded DOX via UV-vis spectrometry. As shown in Table 1, F-G5-PEG/DOX-1 presented the highest drug EE (encapsulation efficiency) (94.5±2.8%) while F-G5-PEG/DOX-3 only yielded 84.5±3.6% drug EE. The higher drug EE of F-G5-PEG/DOX-1 may be explained by the lower TEA to DOX molar ratio resulted in relative lower initial pH that slowed down the formation of dimer or multimer of DOX, thereby affording more time for DOX to assemble inside the PAMAM hydrophobic cavity. It was noteworthy that all of the F-G5-PEG/DOX compositions possessed more competitive drug EE than commercial PAMAM G5 (78.6±4.1%), the higher drug encapsulation efficiency of F-G5-PEG/DOX over G5/DOX might be that the Schiff-base terminals and PEG terminals form a protection shell, which can prevent DOX diffuse freely from dendrimer interior to outside bulk solution.

For antitumor therapeutic applications, the encapsulated DOX should be effectively released into the cytoplasm to reach the nucleus to exert its biological activity. To understand the drug release process, we investigated the cumulative release profile of F-G5-PEG/DOX, in PBS at different pH values (7.2, 6.5, 5.0). The results shown in Fig 5 indicated that DOX was sustainably released from F-G5-PEG/DOX in PBS solution at all pH values for 72 h. In comparison, free DOX drug was ‘burst released’ whereby almost all DOX was released within

2 h. The release of DOX from F-G5-PEG was enhanced by decreasing the pH value, revealing that the F-G5-PEG/DOX is pH sensitive. We further noticed that the drug release kinetics of the three types of F-G5-PEG/DOX were strongly associated with the initial molar ratio of TEA to DOX·HCl, reflecting the different DOX aggregation characteristics of different formulations (Table 1) as the drug release rate was strongly associated with the solubilization of the aggregated molecules and drug diffusion. Additionally, the size of drug loaded nanocarrier will also affect the drug release rate, as smaller sizes have decreased diffusion distance which results in a faster release rate.

Fluorescence spectra can reflect the aggregation state of fluorescent molecules. DOX contains a chromophore composed of three aromatic hydroxyanthraquinonic rings [41], which can be used to monitor interactions with itself or other molecules. As shown in Fig S5, a remarkable decrease in fluorescence intensity of peaks at 550 and 595 nm were observed with the F-G5-PEG/DOX-3 compared to the equivalent amount of free DOX·HCl. This was a typical self-quenching that resulted from increased local concentrations[42]. In F-G5-PEG/DOX-3 composite, a higher TEA to DOX·HCl molar ratio resulted in a relatively higher initial pH, which facilitated dimer or multimer formation of DOX, generating a relative higher DOX local concentration and in turn leading to decreased fluorescence intensity. Meanwhile, the stronger molecular interactions would also result in a relative slower drug solubilization and diffusion rate leading to a slower drug release speed. These considerations mean that fluorescence spectra are valuable tools enabling the prediction of drug release kinetics.

3.5 Intracellular Drug Delivery and Therapeutic Efficacy

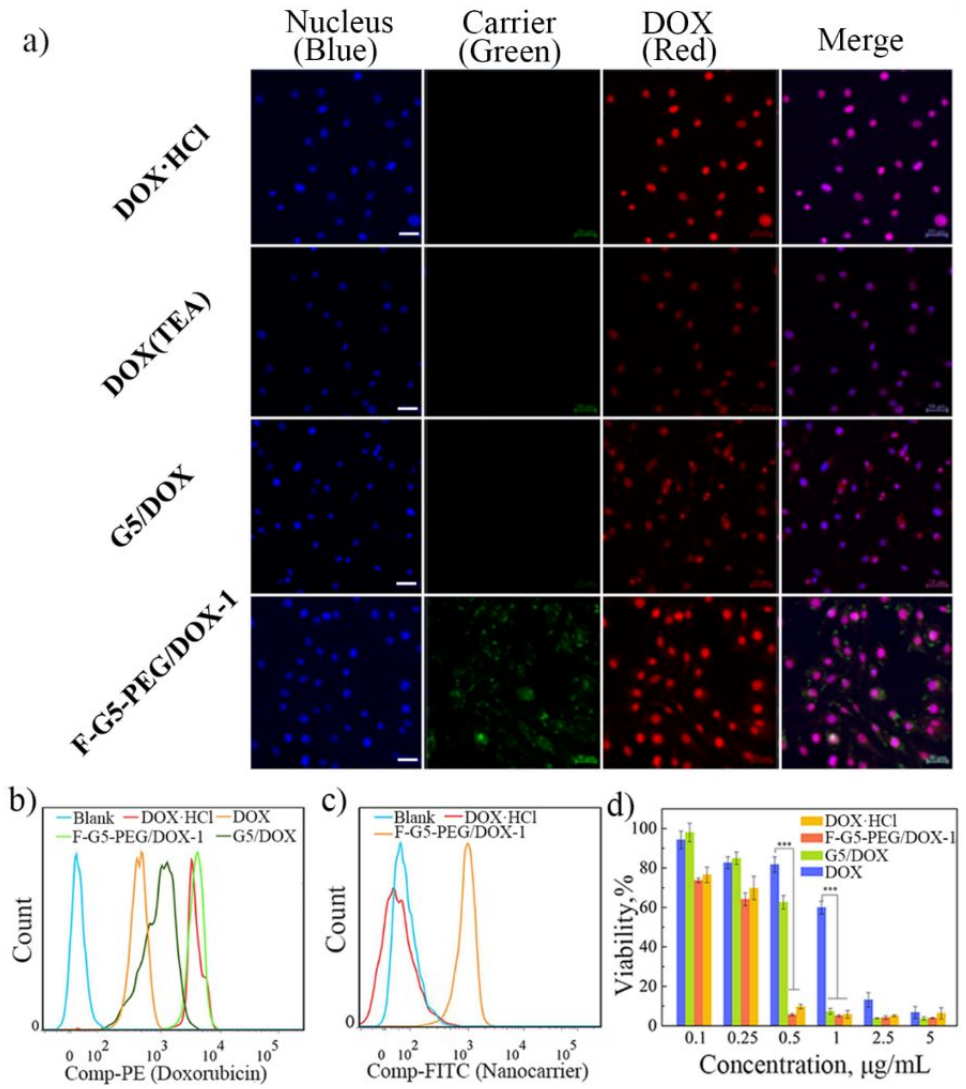

Figure 6. (a) Confocal microscopy images of SKMEL28 cells after 4 h culture in the presence of free DOX·HCl, DOX (TEA treated, hydrophobic DOX), G5/DOX, F-G5-PEG/DOX-1with an equivalent amount of DOX (2.5 μg/mL). Bar =50 μm; (b) (c) Cell cytometry assay of SK MEL 28 cells after 4 h culture in the presence of free DOX·HCl, DOX, G5/DOX, F-G5-PEG/DOX-1with an equivalent amount of DOX (5 μg/mL); (d) Cancer cell cytotoxicity were assessed using SK MEL 28 cells. Free DOX· HCl, DOX (TEA treated), G5/DOX, F-G5-PEG/DOX with an equivalent amount of DOX were added into the cell culture medium, respectively. The cell viability was tested after 48 h incubation with different formulations. (***, $p<0.001$).

Drug carriers should be effectively taken up and deliver active drug into the cells. As DOX is fluorescent (ex/em=490/590), its internalization by SKMEL28 cells can be monitored by fluorescence microscopy. As shown in Fig 6a, no green fluorescence was evident from free DOX or G5/DOX. This confirmed that the green fluorescence must be resulting from the label-free fluorescent nanocarrier. For F-G5-PEG/DOX-1, a much brighter red fluorescence was observed (mostly in the nucleus) compared to hydrophobic DOX or G5/DOX. This higher nuclear DOX accumulation could be mainly attributed to the more efficient cell uptake of the F-G5-PEG/DOX-1 (Fig 6a), as well as enhanced DOX release from the endolysosomal compartments to nucleus as the nanocarrier F-G5-PEG was mainly trapped in the endolysosomal compartments (Fig 4) and the low pH in the endolysosomal compartments facilitated intracellular drug release (Fig 3a). At the same time, from the *in vitro* drug release experiment, it was clearly shown that about 45% DOX released from the F-G5-PEG/DOX-1 during the first 4 hours. This proved that the extra cellular drug release from F-G5-PEG/DOX might also improve the intracellular DOX accumulation. Additionally, the endocytosis of free form hydrophobic DOX was very low, reflecting that the F-G5-PEG/DOX composites indeed improved the solubility of hydrophobic drugs. We further compared the nanocarrier and drug uptake between different F-G5-PEG/DOX compositions via confocal microscopy. The images in Fig S6a showed weaker green and red signals from F-G5-PEG/DOX-2 and F-G5-PEG/DOX-3 treated cells compared to F-G5-PEG/DOX-1 treated cells, indicating less cell uptake of both nanocarrier and drug for F-G5-PEG/DOX-2 and F-G5-PEG/DOX-3. The higher nanocarrier uptake of F-G5-PEG/DOX-1 most likely reflected the relatively smaller size of the particles, which were more easily taken up by the cells. The higher DOX accumulation in nucleus of F-G5-PEG/DOX-1 treatment was most likely attributed to the relatively higher composition uptake and faster drug release from the endolysosomal compartments to nucleus as well as a relative higher extra cellular release of DOX from F-G5-PEG/DOX-1.

Flow cytometry was used to quantitatively study cell uptake of the compounds. As shown in Fig 6b, Fig S6b and Fig S7a, a higher DOX uptake was achieved by F-G5-PEG/DOX-1 compared to free hydrophobic DOX or G5/DOX (5.2 and 3.7times, respectively). Nanocarrier and drug uptake between different F-G5-PEG/DOX compositions were shown in Fig S6b-c and Fig S7a-b, F-G5-PEG/DOX-2 and F-G5-PEG/DOX-3 showed 39.2% and 59.7% less nanocarrier uptake and 46.7% and 60.8% less DOX uptake, respectively than F-G5-PEG/DOX-1. The flow cytometry results showed similar drug and nanocarrier uptake, agreeing with the confocal microscopy results and demonstrated that F-G5-PEG was an efficient drug delivery vehicle for DOX, and F-G5-PEG/DOX-1was the most efficient nanocarrier for *in vitro* intracellular drug accumulation.

The cytotoxicity of the DOX-loaded F-G5-PEG was quantitatively evaluated in SKMel28 cells by MTT assay. As shown in Fig 6d, F-G5-PEG/DOX-1showed enhanced cytotoxicity (IC50=0.174 μg), whereas free hydrophobic DOX induced mild cytotoxicity as expected (IC50=0.903μg) reflecting lower solubility in cell culture media (Fig 6d). Biocompatibility experiments revealed that blank F-G5-PEG did not display any cytotoxicity (Fig 3), thereby demonstrating that cytotoxic effects were only possible when DOX was loaded within the nanocomposites. Most importantly, even at very low DOX concentration (0.5 μg/mL), F-G5-PEG/DOX-1 could still induce an impressive cytotoxic effect (5.7 ± 0.5% cell viability) relative to free hydrophobic DOX drug (87.76 ± 3.9 % cell viability), which was comparable to DOX·HCl molecules. The G5/DOX system showed intermediate cytotoxicity (IC50=0.569 μg) compared with other compositions. Combined with the drug uptake investigation, these results, collectively showed that the cytotoxicity was strongly associated with the degree of DOX uptake by the respective formulations, confirming that the intracellular drug concentration was crucial for mediating cell death. We further compared the cytotoxicity between different F-G5-PEG/DOX compositions, as shown in Fig S8, F-G5-PEG/DOX-1 exhibited the best cancer cell

toxicity (IC50=0.174 μg) while F-G5-PEG/DOX-3 held the weakest cancer cell toxicity (IC50=0.712 μg) and F-G5-PEG/DOX-2 held intermediate cancer cell toxicity (IC50=0.305 μg). The higher therapeutic efficacy of F-G5-PEG/DOX-1 to SKMel28 cells most likely attributed to the higher drug accumulation in nucleus by effective nanocomposite endocytosis, pH enhanced drug release as well as relative fast extra cellular drug release. In this study, the fast extra cellular release of DOX from F-G5-PEG/DOX-1 indeed improved the therapeutic efficacy, however, that may also cause side effects, its valuable if the "burst release" can be avoided. Prospectively, surface cross-linking with biodegradable polymer or surface conjugation with drugs may be effective approaches to prevent the burst drug release from PAMAM/drug delivery system[43, 44]. Supported by our cell uptake data and cancer cell therapeutic data, we have thereby show that the F-G5-PEG/DOX system may be an improved drug delivery system for DOX for cancer treatment and provided guidance for other drug delivery system designs.

4 CONCLUSION

In this study, we successfully produced a new label free fluorescent PAMAM with strong green fluorescence at maximum wavelength ex/em=485/507 nm. The novel fluorescent dendrimer F-G5/F-G5-PEG showed promising biocompatibility and intracellular imaging capability. Anti-cancer drug DOX could be efficiently encapsulated into F-G5-PEG by a solvent-displacement method. It was notable that the drug release characteristics of F-G5-PEG/DOX was pH sensitive and the drug release rate was strongly associated to the initial ratio between TEA and DOX·HCl. Attractively, the F-G5-PEG/DOX system displayed higher cell uptake and more effective therapeutic efficacy than hydrophobic DOX and G5/DOX alone. The high efficiency of this new dendritic drug vehicle suggests that further investigation into their development as carriers is warranted not just for DOX, but also for other clinically important drugs.

SUPPORTING INFORMATION

Chemical and physical characterization of pristine PAMAM, F-G5 and F-G5-PEG by TEM images, FT-IR, 1H NMR and Fluorescence spectrophotometry. Fluorescence spectrum of nanocarrier/DOX nanocomposites. Size distribution of nanocarrier and nanocarrier/DOX nanocomposites. The data for intracellular drug delivery and therapeutic efficacy.

ACKNOWLEDGEMENTS

We gratefully acknowledge the financial support of Mason Foundation (No.MAS2017F034), Endeavour Fellowship (No.69172018), NHMRC-ARC dementia Career Development Research Fellowship (APP1111611), National Natural Science Foundation of China (NSFC 31600809 and U1604177), the National Key Technologies R&D program of China (2018YFA0209800) NHMRC RD Wright Career Development Fellowship (APP 1140386), Ross Maclean Fellowship for MND Research, Brazil Family Program for Neurology, and the International Macquarie University Research Excellence Scholarship (iMQRES).

REFERENCE

(1) Ali, U.; Karim, K. J. B. A.; Buang, N. A. A review of the properties and applications of poly (methyl methacrylate)(PMMA), *Polymer Reviews* **2015,** 55, (4), 678-705.

(2) Saraiva, C.; Praça, C.; Ferreira, R.; Santos, T.; Ferreira, L.; Bernardino, L. Nanoparticle-mediated brain drug delivery: overcoming blood–brain barrier to treat neurodegenerative diseases, *J. Controlled Release* **2016,** 235, 34-47.

(3) Gothwal, A.; Kesharwani, P.; Gupta, U.; Khan, I.; Cairul Iqbal Mohd Amin, M.; Banerjee, S.; K Iyer, A. Dendrimers as an effective nanocarrier in cardiovascular disease, *Curr. Pharm. Des.* **2015,** 21, (30), 4519-4526.

(4) Wang, Y.; Guo, R.; Cao, X.; Shen, M.; Shi, X. Encapsulation of 2-methoxyestradiol within multifunctional poly (amidoamine) dendrimers for targeted cancer therapy, *Biomaterials* **2011,** 32, (12), 3322-3329.

(5) Esfand, R.; Tomalia, D. A. Poly (amidoamine)(PAMAM) dendrimers: from biomimicry to drug delivery and biomedical applications, *Drug discovery today* **2001,** 6, (8), 427-436.

(6) Hsu, H. J.; Bugno, J.; Lee, S. r.; Hong, S. Dendrimer-based nanocarriers: a versatile platform for drug delivery, *Wiley Interdiscip Rev Nanomed Nanobiotechnol* **2017,** 9, (1), e1409.

(7) Liu, Y.; Chiu, G. N. Dual-functionalized PAMAM dendrimers with improved P-glycoprotein inhibition and tight junction modulating effect, *Biomacromolecules* **2013,** 14, (12), 4226-4235.

(8) Fu, F.; Wu, Y.; Zhu, J.; Wen, S.; Shen, M.; Shi, X. Multifunctional lactobionic acid-modified dendrimers for targeted drug delivery to liver cancer cells: investigating the role played by PEG spacer, *ACS applied materials & interfaces* **2014,** 6, (18), 16416-16425.

(9) White, N. S.; Errington, R. J. Fluorescence techniques for drug delivery research: theory and practice, *Adv. Drug Delivery Rev.* **2005,** 57, (1), 17-42.

(10) Watson, P.; Jones, A. T.; Stephens, D. J. Intracellular trafficking pathways and drug delivery: fluorescence imaging of living and fixed cells, *Adv. Drug Delivery Rev.* **2005,** 57, (1), 43-61.

(11) Denora, N.; Laquintana, V.; Lopalco, A.; Iacobazzi, R. M.; Lopedota, A.; Cutrignelli, A.; Iacobellis, G.; Annese, C.; Cascione, M.; Leporatti, S. In vitro targeting and imaging the translocator protein TSPO 18-kDa through G (4)-PAMAM–FITC labeled dendrimer, *J. Controlled Release* **2013,** 172, (3), 1111-1125.

(12) Du, X.; Shi, B.; Tang, Y.; Dai, S.; Qiao, S. Z. Label-free dendrimer-like silica nanohybrids for traceable and controlled gene delivery, *Biomaterials* **2014,** 35, (21), 5580-5590.

(13) Shi, B.; Zhang, H.; Qiao, S. Z.; Bi, J.; Dai, S. Intracellular Microenvironment-Responsive Label-Free Autofluorescent Nanogels for Traceable Gene Delivery, *Adv. Healthcare Mater.* **2014,** 3, (11), 1839-1848.

(14) Lee, W. I.; Bae, Y.; Bard, A. J. Strong blue photoluminescence and ECL from OH-terminated PAMAM dendrimers in the absence of gold nanoparticles, *J. Am. Chem. Soc.* **2004,** 126, (27), 8358-8359.

(15) Wang, D.; Imae, T. Fluorescence emission from dendrimers and its pH dependence, *Journal of the American Chemical Society* **2004,** 126, (41), 13204-13205.

(16) Tomalia, D. A.; Klajnert-Maculewicz, B.; Johnson, K. A.-M.; Brinkman, H. F.; Janaszewska, A.; Hedstrand, D. M. Non-traditional intrinsic luminescence: inexplicable blue fluorescence observed for dendrimers, macromolecules and small molecular structures lacking traditional/conventional luminophores, *Progress in Polymer Science* **2018**.

(17) Tsai, Y.-J.; Hu, C.-C.; Chu, C.-C.; Imae, T. Intrinsically fluorescent PAMAM dendrimer as gene carrier and nanoprobe for nucleic acids delivery: bioimaging and transfection study, *Biomacromolecules* **2011,** 12, (12), 4283-4290.

(18) Yang, W.; Pan, C.-Y.; Luo, M.-D.; Zhang, H.-B. Fluorescent mannose-functionalized hyperbranched poly (amido amine) s: synthesis and interaction with E. coli, *Biomacromolecules* **2010,** 11, (7), 1840-1846.

(19) Jiang, T.; Jiang, G.; Wang, X.; Dong, Y.; Wei, Z.; Li, X.; Tang, B. Facile one-pot synthesis of fluorescent hyperbranched polymers for optical detection of glucose, *Designed Monomers and Polymers* **2014,** 17, (6), 576-581.

(20) Janaszewska, A.; Studzian, M.; Petersen, J. F.; Ficker, M.; Paolucci, V.; Christensen, J. B.; Tomalia, D. A.; Klajnert-Maculewicz, B. Modified PAMAM dendrimer with 4-carbomethoxypyrrolidone surface groups-its uptake, efflux, and location in a cell, *Colloids and Surfaces B: Biointerfaces* **2017,** 159, 211-216.

(21) Pérez-Sánchez, A.; Barrajón-Catalán, E.; Caturla, N.; Castillo, J.; Benavente-García, O.; Alcaraz, M.; Micol, V. Protective effects of citrus and rosemary extracts on UV-induced damage in skin cell model and human volunteers, *J. Photochem. Photobiol., B* **2014,** 136, 12-18.

(22) Monici, M. Cell and tissue autofluorescence research and diagnostic applications, *Biotechnol. Ann. Rev.* **2005,** 11, 227-256.

(23) Kim, H. M.; Noh, Y. W.; Park, H. S.; Cho, M. Y.; Hong, K. S.; Lee, H.; Shin, D. H.; Kang, J.; Sung, M. H.; Poo, H. Self-Fluorescence of Chemically Crosslinked MRI Nanoprobes to Enable Multimodal Imaging of Therapeutic Cells, *Small* **2012,** 8, (5), 666-670.

(24) Jevprasesphant, R.; Penny, J.; Jalal, R.; Attwood, D.; McKeown, N.; D'emanuele, A. The influence of surface modification on the cytotoxicity of PAMAM dendrimers, *Int. J. Pharm.* **2003,** 252, (1), 263-266.

(25) Luong, D.; Kesharwani, P.; Deshmukh, R.; Amin, M. C. I. M.; Gupta, U.; Greish, K.; Iyer, A. K. PEGylated PAMAM dendrimers: Enhancing efficacy and mitigating toxicity for effective anticancer drug and gene delivery, *Acta Biomater.* **2016,** 43, 14-29.

(26) Li, Y.; He, H.; Lu, W.; Jia, X. A poly (amidoamine) dendrimer-based drug carrier for delivering DOX to gliomas cells, *RSC Adv* **2017,** 7, (25), 15475-15481.

(27) Yu, H.; Nie, Y.; Dohmen, C.; Li, Y.; Wagner, E. Epidermal growth factor–PEG functionalized PAMAM-pentaethylenehexamine dendron for targeted gene delivery produced by click chemistry, *Biomacromolecules* **2011,** 12, (6), 2039-2047.

(28) Wang, Y.; Cao, X.; Guo, R.; Shen, M.; Zhang, M.; Zhu, M.; Shi, X. Targeted delivery of doxorubicin into cancer cells using a folic acid–dendrimer conjugate, *Polymer Chemistry* **2011,** 2, (8), 1754-1760.

(29) He, X.; Alves, C. S.; Oliveira, N.; Rodrigues, J.; Zhu, J.; Banyai, I.; Tomas, H.; Shi, X. RGD peptide-modified multifunctional dendrimer platform for drug encapsulation and targeted inhibition of cancer cells, *Colloids Surf. B. Biointerfaces* **2015,** 125, 82-89.

(30) Abedi-Gaballu, F.; Dehghan, G.; Ghaffari, M.; Yekta, R.; Abbaspour-Ravasjani, S.; Baradaran, B.; Dolatabadi, J. E. N.; Hamblin, M. R. PAMAM dendrimers as efficient drug and gene delivery nanosystems for cancer therapy, *Appl Mater Today* **2018,** 12, 177-190.

(31) Patri, A. K.; Kukowska-Latallo, J. F.; Baker Jr, J. R. Targeted drug delivery with dendrimers: comparison of the release kinetics of covalently conjugated drug and non-covalent drug inclusion complex, *Adv. Drug Deliv. Rev.* **2005,** 57, (15), 2203-2214.

(32) Xavier, A.; Srividhya, N. Synthesis and study of Schiff base ligands, *IOSR Journal of Applied Chemistry* **2014,** 7, (11), 06-15.

(33) Shi, B.; Zhang, H.; Dai, S.; Du, X.; Bi, J.; Qiao, S. Z. Intracellular microenvironment responsive polymers: a multiple-stage transport platform for high-performance gene delivery, *Small* **2014,** 10, (5), 871-877.

(34) Peng, Z.; Li, H.; Ba, X.; Zhao, J.; Sun, X.; Li, Y. Synthesis of TiO2 nanoparticles in the PAMAM hydrogen network template, *e-Polymers* **2016,** 16, (3), 177-180.

(35) Michen, B.; Geers, C.; Vanhecke, D.; Endes, C.; Rothen-Rutishauser, B.; Balog, S.; Petri-Fink, A. Avoiding drying-artifacts in transmission electron microscopy: Characterizing the size and colloidal state of nanoparticles, *Scientific reports* **2015,** 5, 9793.

(36) Kolhatkar, R. B.; Kitchens, K. M.; Swaan, P. W.; Ghandehari, H. Surface acetylation of polyamidoamine (PAMAM) dendrimers decreases cytotoxicity while maintaining membrane permeability, *Bioconjugate Chem.* **2007,** 18, (6), 2054-2060.

(37) Cheng, L.; Hu, Q.; Cheng, L.; Hu, W.; Xu, M.; Zhu, Y.; Zhang, L.; Chen, D. Construction and evaluation of PAMAM–DOX conjugates with superior tumor recognition and intracellular acid-triggered drug release properties, *Colloids Surf., B* **2015,** 136, 37-45.

(38) Sanson, C.; Schatz, C.; Le Meins, J.-F.; Soum, A.; Thévenot, J.; Garanger, E.; Lecommandoux, S. A simple method to achieve high doxorubicin loading in biodegradable polymersomes, *J. Controlled Release* **2010,** 147, (3), 428-435.

(39) Guerrini, L.; Alvarez-Puebla, R.; Pazos-Perez, N. Surface Modifications of Nanoparticles for Stability in Biological Fluids, *Materials* **2018,** 11, (7), 1154.

(40) Veronese, F. M.; Pasut, G. PEGylation, successful approach to drug delivery, *Drug Discovery Today* **2005,** 10, (21), 1451-1458.

(41) Yin, H.; Bae, Y. H. Physicochemical aspects of doxorubicin-loaded pH-sensitive polymeric micelle formulations from a mixture of poly (L-histidine)-b-poly (L-lactide)-b-poly (ethylene glycol), *Eur J Pharm Biopharm* **2009,** 71, (2), 223-230.

(42) Jang, W. D.; Nishiyama, N.; Zhang, G. D.; Harada, A.; Jiang, D. L.; Kawauchi, S.; Morimoto, Y.; Kikuchi, M.; Koyama, H.; Aida, T. Supramolecular nanocarrier of anionic dendrimer porphyrins with cationic block copolymers modified with polyethylene glycol to enhance intracellular photodynamic efficacy, *Angew. Chem. Int. Ed.* **2005,** 44, (3), 419-423.

(43) Hezaveh, H.; Muhamad, I. I. Controlled drug release via minimization of burst release in pH-response kappa-carrageenan/polyvinyl alcohol hydrogels, *Chem. Eng. Res. Des.* **2013,** 91, (3), 508-519.

(44) Zhang, M.; Zhu, J.; Zheng, Y.; Guo, R.; Wang, S.; Mignani, S.; Caminade, A.-M.; Majoral, J.-P.; Shi, X. Doxorubicin-conjugated PAMAM dendrimers for pH-responsive drug release and folic acid-targeted cancer therapy, *Pharmaceutics* **2018,** 10, (3), 162.

Table of Contents (TOC) graphic

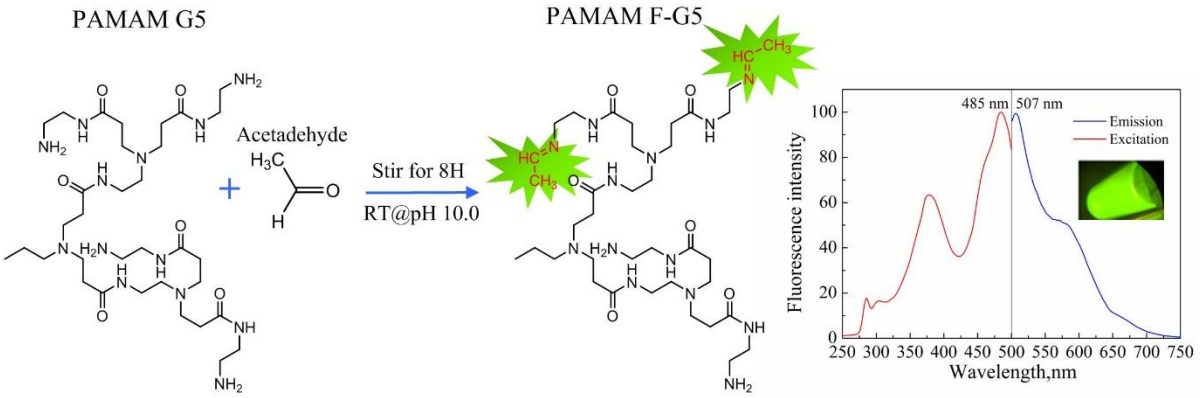

Inherent green fluorescence PAMAM G5